PHYSICAL REVIEW C VOLUME 40, NUMBER 2 AUGUST 1989

Determination of the impact vector in intermediate energy heavy ion collisions

C. A. Ogilvie, D. A. Cebra, J. Clayton, S. Howden, J. Karn, A. Vander Molen,
G. D. Westfall, W. K. Wilson, and J. S. Winfield
National Superconducting Cyclotron Laboratory and Department of Physics and Astronomy, Michigan State University, East Lansing, Michigan 48824
(Received 13 March 1989)

We examine a variety of methods for determining both the impact parameter and the direction of the impact vector in symmetric nuclear collisions at intermediate energies. Two quantities, the particle multiplicity and the midrapidity charge, retain their dependence on the impact parameter after filtering through the acceptance of a typical 4π detector. By gating on these quantities we can select four ranges of impact parameters. There is some overlap of these ranges. It is noted that this is dependent on the model used to simulate the collisions. The midrapidity charge has the advantage that it integrates over the final fragments and should be less sensitive to how the collision zone disassembles. The angle of the impact vector is well reproduced with the method developed by Danielewicz and Odyniec. The difference between known and determined reaction plane has a half-width at half-maximum of less than 70°. Some comparisons are made to experimental data.

I. INTRODUCTION

To unravel the complex processes that occur during nuclear collisions it is necessary to have a reaction mechanism filter; one that separates the central collisions from the grazing collisions, with some differentiation for the midimpact collisions. By gating on the impact parameter, one can begin to answer questions such as how do the thermodynamic properties of the collision zone depend on the violence of the collision. Some quantities of interest also require a measurement of the direction of the impact vector. For example, the measurement of the collective flow produced in collisions[1] requires a determination of the reaction plane; i.e., the plane defined by the impact vector and the beam axis.

The aim of this paper is to study how well the impact vector can be determined experimentally in intermediate-energy heavy-ion collisions. For these energies this can be done by two distinct methods. The first relates the folding angle of fission fragments to the impact parameter, while the second utilizes global variables.

In the first method,[2–5] a light projectile bombards a heavy target whose residue fissions after the collision process. The folding angle of the two fission fragments depends on the linear momentum of the parent targetlike nucleus. This momentum is transferred during the collision and is expected to increase the more central the collision. Thus one can infer the impact parameter from the measured folding angle. The direction of the impact vector is deduced from the azimuthal angle of the fission fragments. The fission products are preferentially emitted perpendicular to the angular momentum vector of the parent. This vector, in turn, is perpendicular to the impact vector. Note that this means that the sign of the impact vector is undetermined. There are several problems with this reaction filter: (1) its use is restricted to targets whose residues will fission and (2) as the beam energy increases the probability of the target residue fissioning into only two fragments decreases.[6] There are no simulations in the published literature that show how accurately this method determines the impact vector.

In the second method, one measures as many of the reaction products as is possible. Quantities derived from the measured products such as the multiplicity, or momentum distribution, may be sensitive enough to the impact parameter to be used as a reaction filter. Ideally such quantities should not depend on the fine details of the model used to calculate the reaction. This technique has been used by the Plastic Ball group[7] for higher energy collisions. For the Plastic Ball and other data, Danielewicz and Odyniec[8] have demonstrated that the direction of the impact vector can be determined from the momentum distribution of the reaction products. This method is subject to fluctuations due the presence of thermal energy generated during the collision and due to the finite multiplicity of the particles.

It is this second method of finding a reaction filter that we investigate here. In Sec. II the various derived quantities are introduced and then used in Sec. III as we consider symmetric collisions of $A=40$ nuclei. In Sec. IV we compare some of our results to experiment and in Sec. V we present our conclusions.

II. IMPACT-PARAMETER-DEPENDENT QUANTITIES, MODEL CALCULATIONS, AND DETECTOR SIMULATION

We have simulated heavy-ion collisions with the statistical event generator FREESCO.[9] The code uses a modified fireball prescription to generate four thermal sources, the size of which depend on the impact parameter. There are two equal size participant sources with opposite transverse momenta, and two spectator sources also with some transverse momenta and some thermal energy acquired from the participants. The FREESCO pa-

rameters x_0, y_0, z_0, and χ govern the excitation energy and momenta of the sources and are explained in Ref. 9. Throughout this work we use the default parameters of $x_0=0.2$, $y_0=e^{-\sqrt{E_{\text{per}}N/125\ \text{MeV}}}$, $z_0=0.2$, and $\chi=1$. The four sources then de-excite via explosion and evaporation. The dynamics of this model may be somewhat inadequate at the bombarding energies considered here ($E\leq 100$ MeV/nucleon), but the main advantage of FREESCO is that it provides the full range of possible fragments. Other models contain more detailed dynamics but can only produce nucleons or test particles, e.g., the Vlasov-Uhling-Uhlenbeck model (VUU).[10] FREESCO provides an event-by-event simulation of the nuclear collisions, and from the final fragments we can construct several observables that are likely to depend on the impact parameter.

(i) *Particle multiplicity.* As the impact parameter is reduced, more kinetic energy will be transferred to the internal energy of the colliding system. With high internal energy, the system is likely to disintegrate into more fragments. The physics of this disassembly is not fully understood, which means that the particle multiplicity is dependent on the fine details of the assumed model.

(ii) *Backward and forward particle multiplicity.* Backward is here defined to be $\theta_{\text{lab}}>20°$ and forward is $\theta_{\text{lab}}<20°$. Peripheral collisions are expected to produce very few particles at large angles, compared to more central collisions. Recently Tsang *et al.*[11] have shown that, for asymmetric collisions, the forward multiplicity does not correlate with the folding angle of fission fragments. A correlation was observed for the backward multiplicity.

(iii) *Beam direction diagonal component of the quadrupole momentum tensor (Q_{zz}).* Recently[12] this quantity has been proposed as a measure of the impact parameter. For central collisions Q_{zz} is zero since the momentum distribution is symmetric in the center-of-mass frame. It is predicted to monotonically increase with increasing impact parameter.

(iv) *Total perpendicular momentum ($P_\perp$).* This quantity is often used in high energy collisions. It is the total transverse momentum of all the particles in the event and is thereby related to the removal of kinetic energy from the beam direction. From high energy work, we expect $P_\perp$ to increase with smaller impact parameters.

(v) *Midrapidity charge.* In symmetric collisions one expects the participant volume to increase with decreasing impact parameter. Integrating the charge of those particles that have rapidities y between $0.75\times y_{\text{c.m.}}^{\text{target}}$ and $0.75\times y_{\text{c.m.}}^{\text{proj}}$ could provide a measure of the collision zone. Because of the integration, the midrapidity charge is expected to be relatively insensitive to how the participant zone disassembles. This quantity is similar to the baryon charge multiplicity used in the Plastic Ball experiments.[7]

The angle of the impact vector **b** can be found using the method developed by Danielewicz and Odyniec.[8] Assuming there exists some collective transverse momentum in the reaction plane, then the vector **Q**

$$\mathbf{Q}=\sum_{\nu=1}^{n}\omega_\nu \mathbf{p}_\nu^\perp \tag{1}$$

will lie in the reaction plane. The sum runs over all the fragments, ω_ν is a weighting factor that has an opposite sign for particles emitted in the forward and backward hemispheres in the c.m., and $\mathbf{p}_\nu^\perp$ is the fragment's perpendicular momentum.

If the dynamics of the reaction cause the collective transverse momentum to resemble repulsive scattering, then **Q** will be parallel to **b**. If the dynamics are dominated by attractive scattering then **Q** will be antiparallel to **b**. The weights ω_ν can be chosen to optimize the accuracy with which the reaction plane is determined. The original work[8] used weights of ± 1 for fragments emitted in the forward and backward hemispheres in the c.m., respectively. In addition to this choice, we will also use the beam direction component of the fragment's c.m. momentum (p^z) as the weighting factor ω_ν. We will compare in Sec. III how accurately these weighting schemes reproduce the reaction plane.

Each of the impact parameter quantities and the direction of the impact vector were calculated for the full events as predicted by the simulation (both neutrons and charged particles). These events were then filtered by the response of a 4π array and the quantities recalculated. As a representative of such an experimental device, a software replica of the 4π array at Michigan State University (MSU) (Ref. 13) was used to filter the events. The device has 45 phoswich detectors in a forward array between $\theta=7°$ and $\theta=20°$, and 170 phoswich detectors in the ball between $\theta=20°$ and $\theta=160°$. The solid angle coverage of the device is 85% of 4π. The software filter includes the low-energy thresholds ($\simeq 12$ MeV/nucleon for the forward array and $\simeq 20$ MeV/nucleon for the ball detectors), the finite angular resolution of the device, the rejection of multiple hits within one detector, the known gaps where particles would not be detected, and shadowing due to the target mechanism. The forward array and ball detectors can measure particles with $Z\leq 8$ and $Z\leq 4$, respectively, and both can provide isotopic resolution for $Z=1$ particles. Higher charged nuclei are assigned $A=2\times Z$. Particles within these Z ranges that stop in ΔE of each detector can be assigned a Z and an approximate energy. These particles are only used to calculate the multiplicity and midrapidity charge. For the filtered simulations we can add a pseudoparticle which consists of the mass, charge, and momentum that was not detected. This pseudo particle will be used for the evaluation of Q_{zz}.

III. ^{40}Ca+^{40}Ca COLLISIONS

We have simulated ^{40}Ca on ^{40}Ca collisions at bombarding energies of 40, 70, and 100 MeV/nucleon with the program FREESCO. Approximately 30 000 collisions were simulated for each energy. The results are shown in Figs. 1–6, where the error bars represent the one standard deviation width of the distribution for each impact parameter bin, b, and $b_{\text{max}}=r_{\text{proj}}+r_{\text{target}}$.

Figure 1 displays the impact parameter dependence of the predicted multiplicity and the filtered multiplicity after passing through the detector's acceptance. Both the predicted and filtered multiplicity increase with bombarding energy and are monotonically dependent on the im-

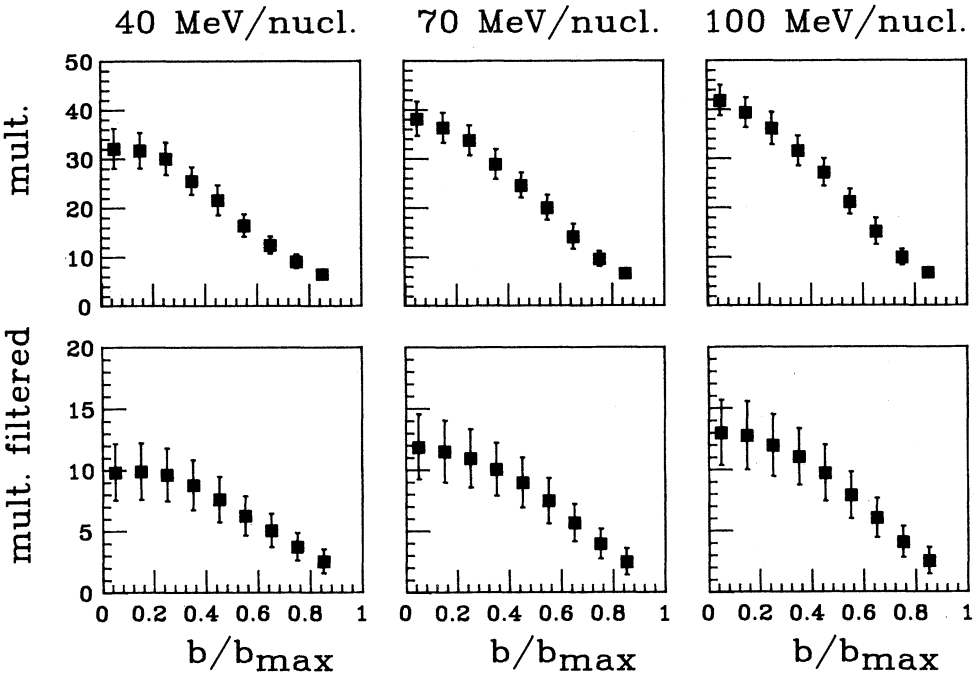

FIG. 1. The dependence of particle multiplicity on the impact parameter for $^{40}Ca+^{40}Ca$ at 40, 70, and 100 MeV/nucleon. The top and bottom panels correspond to the unfiltered and filtered results, respectively. The data points represent the mean values and the error bars represent the one standard deviation width at each impact parameter.

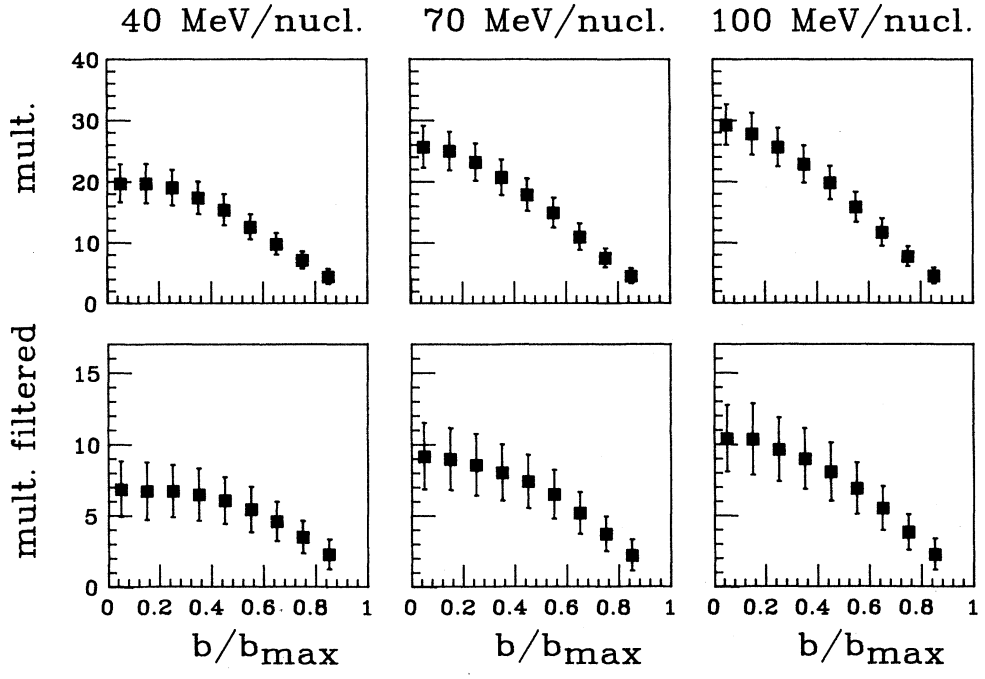

FIG. 2. The dependence of backward particle multiplicity on the impact parameter for $^{40}Ca+^{40}Ca$ at 40, 70, and 100 MeV/nucleon. Backward is defined to be $\theta_{lab} > 20°$.

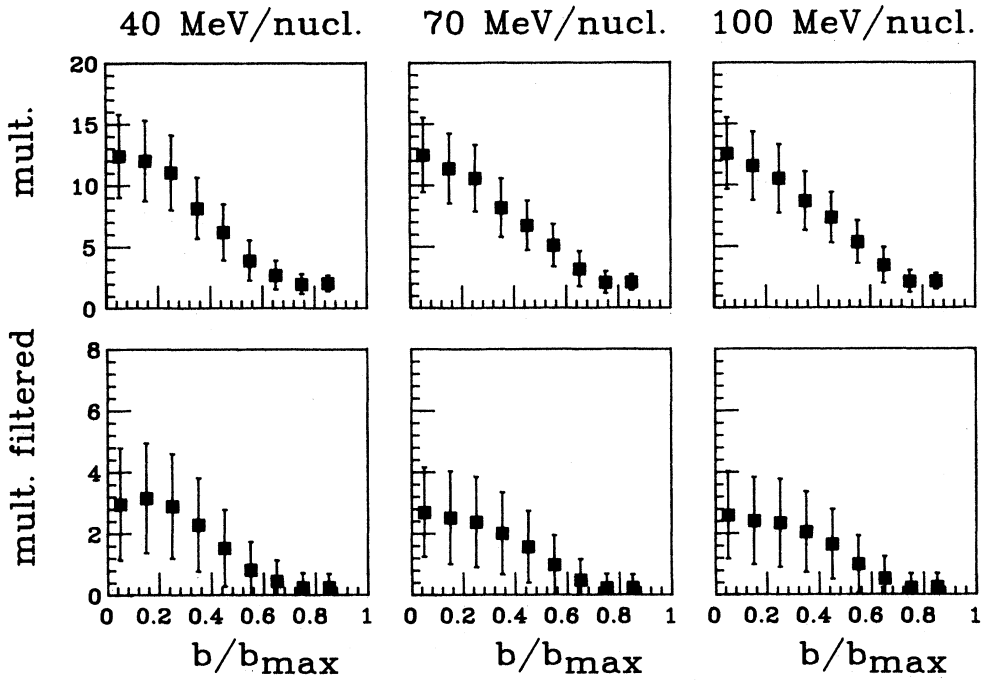

FIG. 3. The dependence of forward particle multiplicity on the impact parameter for $^{40}Ca+^{40}Ca$ at 40, 70, and 100 MeV/nucleon. Forward is defined to be $\theta_{lab} < 20°$.

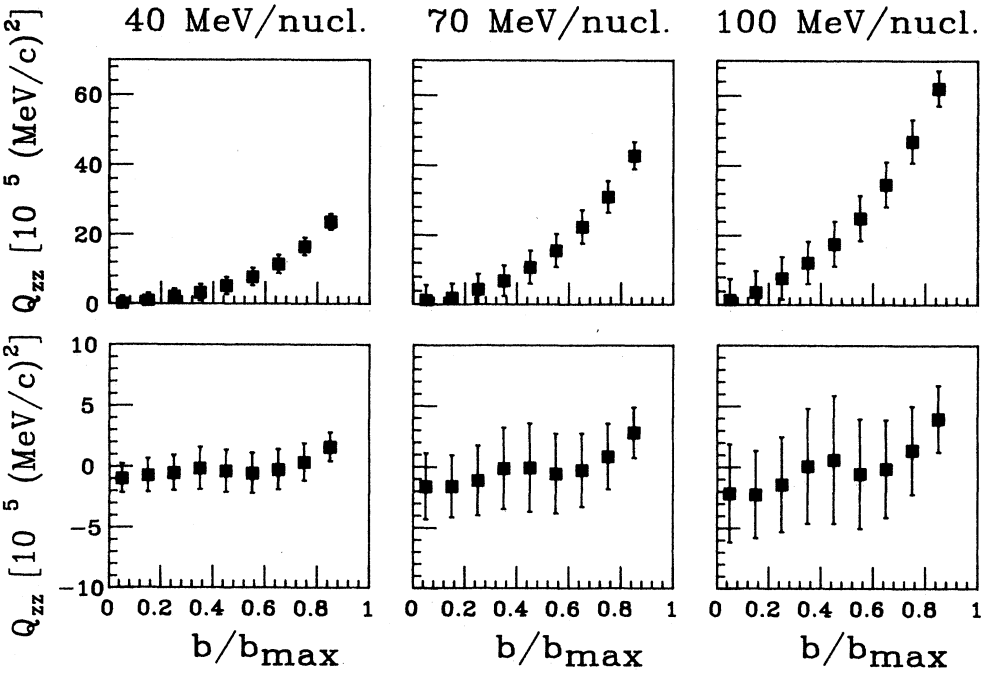

FIG. 4. The dependence of Q_{zz} on the impact parameter for $^{40}Ca+^{40}Ca$ at 40, 70, and 100 MeV/nucleon.

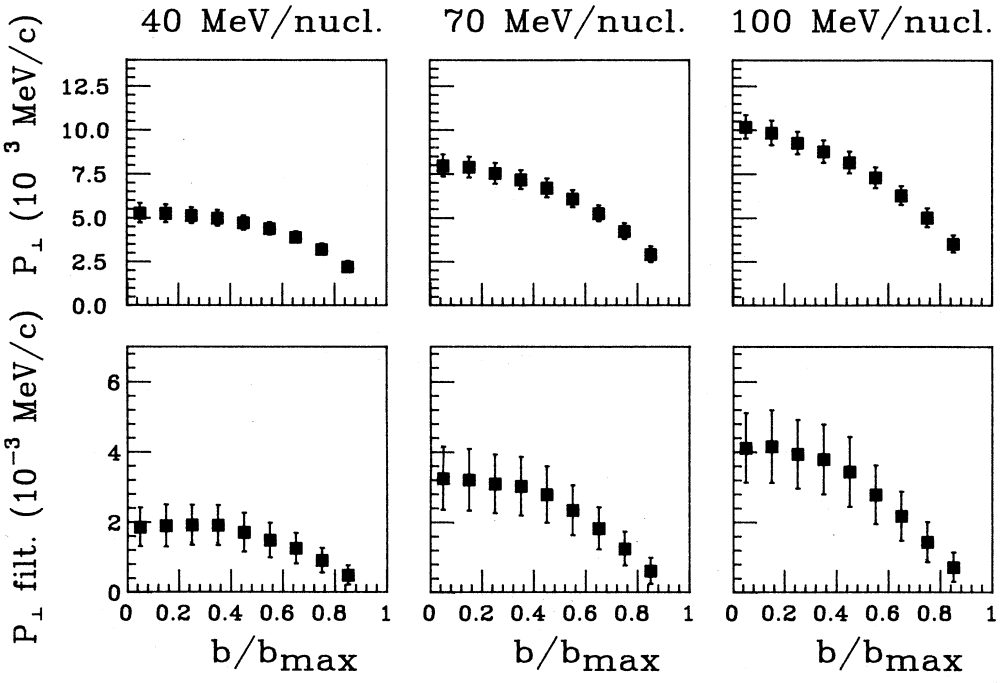

FIG. 5. The dependence of the total perpendicular momentum ($P_\perp$) on the impact parameter for ^{40}Ca+^{40}Ca at 40, 70, and 100 MeV/nucleon.

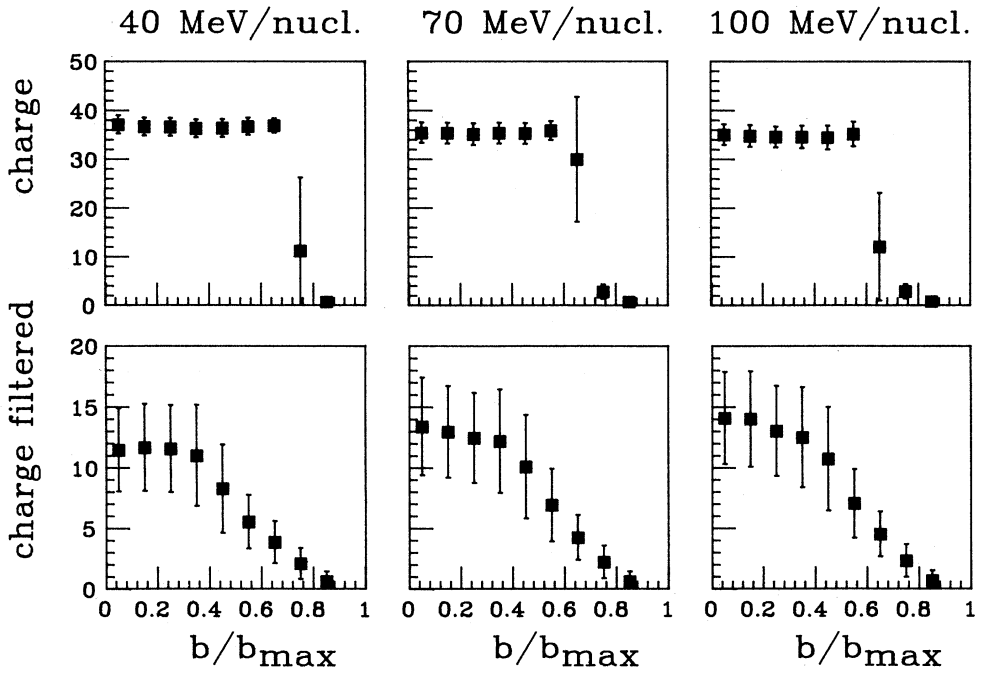

FIG. 6. The dependence of midrapidity charge on the impact parameter for ^{40}Ca+^{40}Ca at 40, 70, and 100 MeV/nucleon.

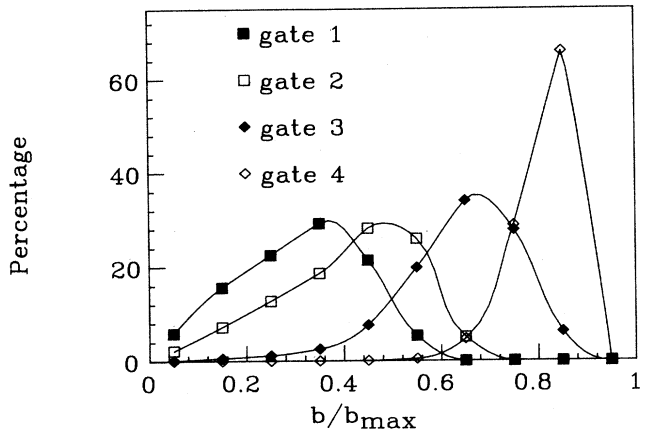

FIG. 7. The percentage of events within each midrapidity charge gate (see Table I) that have a given impact parameter. The system is $^{40}Ca+^{40}Ca$ at 70 MeV/nucleon after filtering through the acceptance of a 4π detector. The lines through the points are to guide the eye and have been found by a three-point smoothing algorithm.

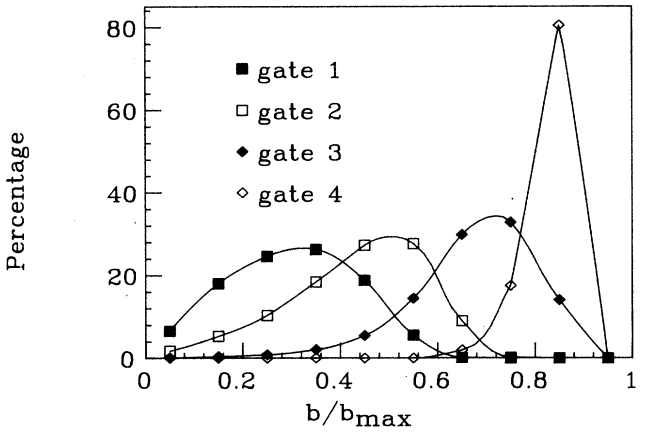

FIG. 8. The percentage of events within each multiplicity gate (see Table II) that have a given impact parameter. The system is $^{40}Ca+^{40}Ca$ at 70 MeV/nucleon after filtering through the acceptance of a 4π detector.

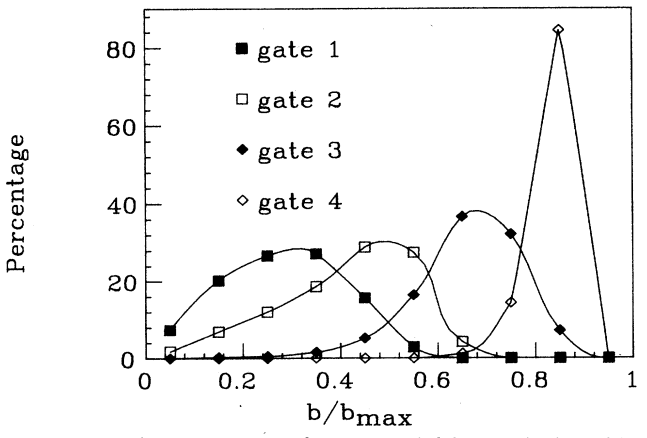

FIG. 9. The percentage of events satisfying both the midrapidity charge and the multiplicity gates that have a given impact parameter. The system is $^{40}Ca+^{40}Ca$ at 70 MeV/nucleon after filtering through the acceptance of a 4π detector.

TABLE I. The gates on midrapidity charge (Z) used to select impact parameter ranges ($^{40}Ca+^{40}Ca$).

	Energy (MeV/nucleon)		
Gate	40	70	100
1	$Z \geq 11$	$Z \geq 12$	$Z \geq 13$
2	$7 \leq Z < 11$	$8 \leq Z < 12$	$9 \leq Z < 13$
3	$2 \leq Z < 7$	$2 \leq Z < 8$	$2 \leq Z < 9$
4	$0 \leq Z < 2$	$0 \leq Z < 2$	$0 \leq Z < 2$

pact parameter. This dependence flattens out for small impact parameters, especially for the lowest beam energy considered here.

The qualitative behavior for the backward multiplicity (Fig. 2) is similar to the total multiplicity but with a larger spread in the distribution for each value of b. The filtered backward multiplicity at 40 MeV/nucleon is independent of b for $0.0 < (b/b_{max}) < 0.5$.

The dependence of the forward multiplicity as a function of b is shown in Fig. 3. Before filtering there is a stronger dependence than for the backward multiplicity, although the width of the distribution is somewhat larger. After filtering this dependence is significantly weakened and there are large fluctuations because of the small number of particles detected.

Figure 4 is a plot of Q_{zz} vs the impact parameter. Before filtering there is a monotonic relationship that is not retained after filtering. This is because the low-energy, low-Z thresholds of the detectors exclude a significant portion of the target residues. Similarly, many projectile residues are excluded because of the Z threshold and because the detector does not span very small angles ($\theta_{lab} \leq 7°$).

As may be seen in Fig. 5, the dependence of $P_\perp$ on the impact parameter is weak even for the unfiltered events. Some sensitivity to b is observed for the highest energy considered here.

The dependence of the midrapidity charge resembles a step function for the unfiltered data (Fig. 6). For collisions with $b < 0.7 \times b_{max}$, the projectile and target spectators lose sufficient center-of-mass kinetic energy to fall within the midrapidity window. The array's Z and E thresholds reduce the effect of these spectators, leaving a dependence on b that is likely to be caused by the changing size of the participant zone. The filtered midrapidity charge increases more steeply as a function of b than the total multiplicity, although the width of the distribution is correspondingly wider.

In the analysis of an experiment, gates that are placed on either the midrapidity charge or the multiplicity will

TABLE II. The gates on multiplicity (M) used to select impact parameter ranges ($^{40}Ca+^{40}Ca$).

	Energy (MeV/nucleon)		
Gate	40	70	100
1	$M \geq 9$	$M \geq 11$	$M \geq 12$
2	$7 \leq M < 9$	$8 \leq M < 11$	$9 \leq M < 12$
3	$3 \leq M < 7$	$3 \leq M < 8$	$3 \leq M < 9$
4	$1 \leq M < 3$	$1 \leq M < 3$	$1 \leq M < 3$

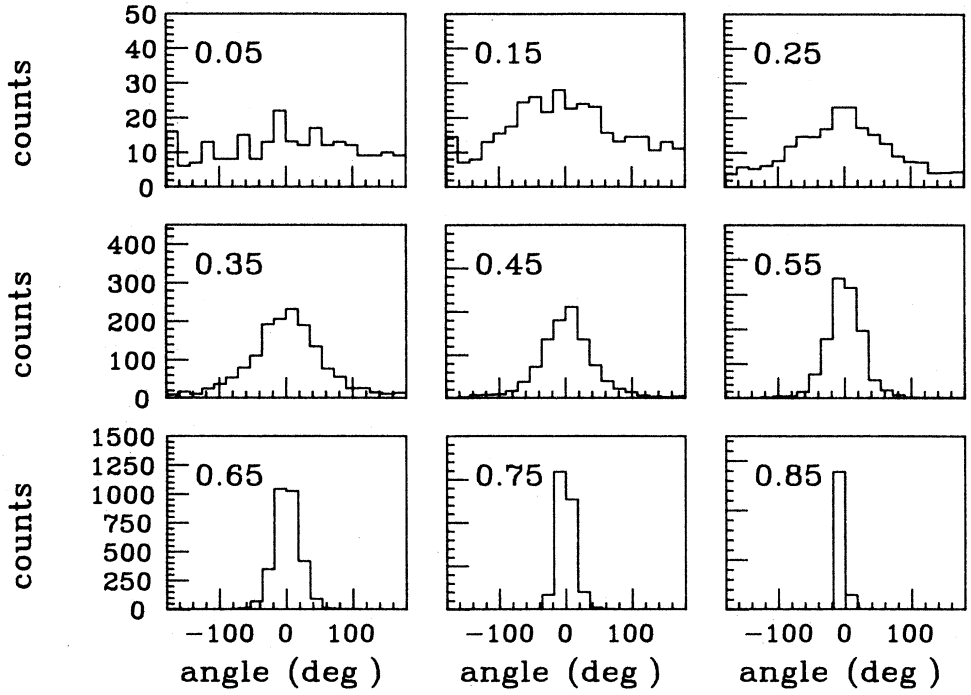

FIG. 10. The difference between the angles of **b** and **Q** for $^{40}Ca+^{40}Ca$ at 70 MeV/nucleon before filtering. The weights used for **Q** were $\omega_\nu=\pm 1$, and the impact parameter bin (b/b_{max}) is given in the upper left corner.

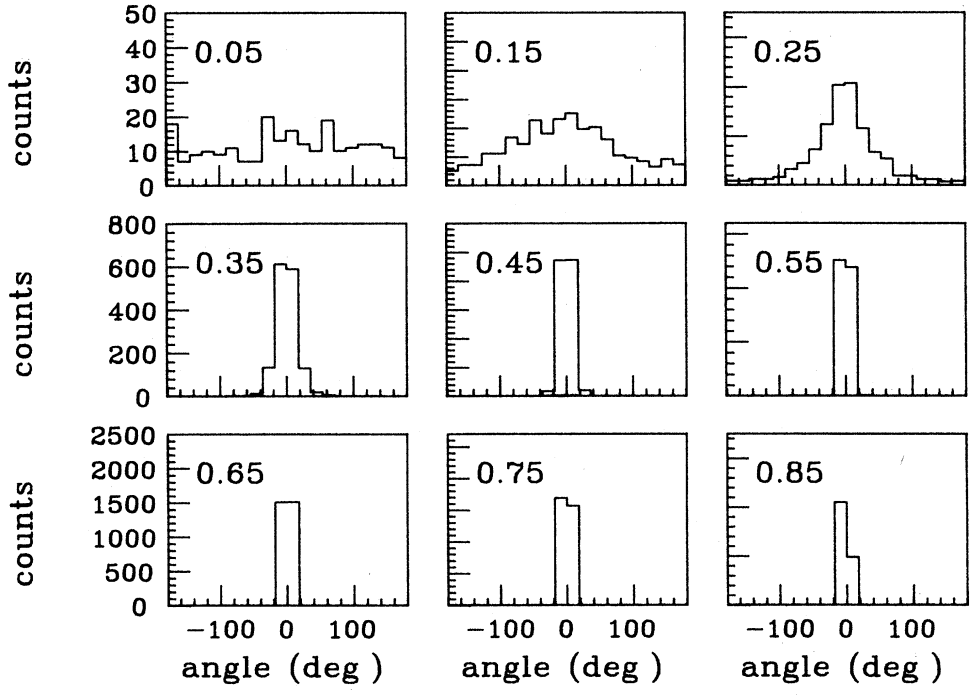

FIG. 11. The difference between the angles of **b** and **Q** for $^{40}Ca+^{40}Ca$ at 70 MeV/nucleon before filtering. The weights used for **Q** were $\omega_\nu=p_\nu^z$, and the impact parameter bin (b/b_{max}) is given in the upper left corner.

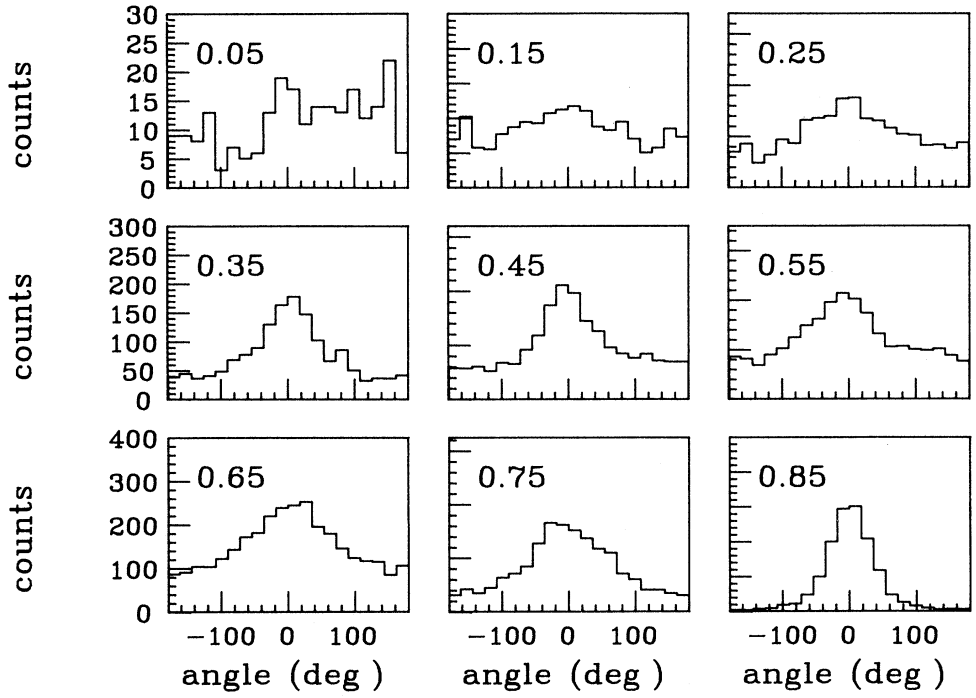

FIG. 12. The difference between the angles of **b** and **Q** for ^{40}Ca+^{40}Ca at 70 MeV/nucleon after filtering. The weights used for **Q** were $\omega_\nu = p_\nu^z$, and the impact parameter bin ($b/b_{\max}$) is given in the upper left corner.

select out events that span a range of impact parameters. The gates listed in Table I for the filtered midrapidity charge produce the sampled impact parameter ranges shown in Fig. 7 for 70 MeV/nucleon. The behavior is similar for the other two energies. This figure shows the percentage of events within each gate that have a given impact parameter. The range sampled is due to the width of the midrapidity charge dependence on impact parameter, weighted by the probability for a collision of a given impact parameter. This probability is proportional to b.

Figure 8 shows the sampled impact parameters for the filtered multiplicity at 70 MeV/nucleon. The gates are listed in Table II and the distributions for 40 and 100 MeV/nucleon are similar. The impact parameter ranges sampled are nearly identical to those obtained for the midrapidity charge. Requiring events to simultaneously satisfy both the midrapidity charge and the multiplicity gates slightly narrows the distribution of sampled impact parameters. This is shown in Fig. 9 for 70 MeV/nucleon.

In FREESCO the angle of the impact vector is known and the collective transverse momentum is directed such that the collisions resemble repulsive scattering. Therefore if **Q** (defined in Sec. II) accurately reproduces the reaction plane it will lie parallel to **b**. In Fig. 10 we plot the difference in angle between the vectors $\hat{\mathbf{b}}$ and $\hat{\mathbf{Q}}$ for ^{40}Ca+^{40}Ca at 70 MeV/nucleon before filtering. The weights used for **Q** were $\omega_\nu = \pm 1$ as described in Sec. II. For midimpact parameters and peripheral collisions the difference between these angles has a maximum at 0°. For small impact parameters FREESCO produces less collective transverse momentum and the thermal motion of the fragments from the hot sources destroys the memory of the already weakly defined reaction plane. As seen in Fig. 11, the weights $\omega_\nu = p_\nu^z$ more accurately reproduce the direction of **b**. We will use this weighting throughout this work.

After filtering through the 4π's acceptance, the difference in angles between **Q** and **b** still has a maximum at 0°. The width of this distribution varies for the different impact parameters and is never greater than a half-width at half-maximum of 70° for $b > 0.25 \times b_{\max}$. This is seen for 70 MeV/nucleon in Fig. 12. The results are similar for 40 and 100 MeV/nucleon.

IV. COMPARISON TO EXPERIMENT

It is not possible to directly compare the impact dependence of the quantities described in this paper with experiment. However the inclusive experimental yield of a quantity should reflect whether it is well modeled over the full range of impact parameters. This is demonstrated in Fig. 13 where we plot the yield of midrapidity charge for the system ^{40}Ar+^{51}V at 35 MeV/nucleon. The experiment was performed with the MSU 4π Array using a beam from the National Superconducting Cyclotron Laboratory's (NSCL) K500 cyclotron, and full details will be given in a later publication.[14] The calculation shown in Fig. 13 uses the code FREESCO and the 4π filter described in Sec. II. The agreement between data and theory is reasonable.

A second comparison to experiment is to examine the kinetic energy spectrum of a particle gated on the impact parameter. The contribution of the projectilelike source

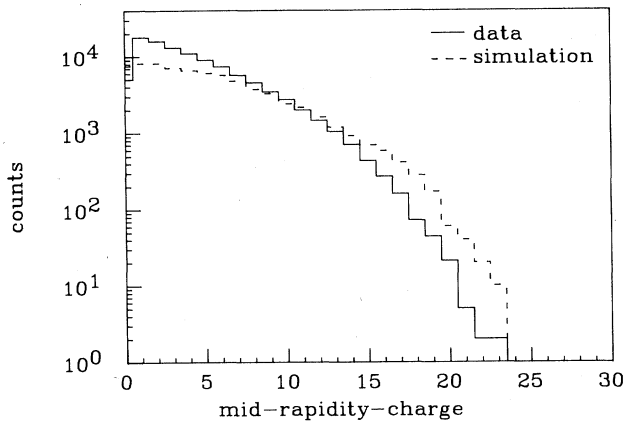

FIG. 13. A comparison of experimental (solid line) and simulated (dashes) yields of the midrapidity charge for the reaction $^{40}Ar+^{51}V$ at 35 MeV/nucleon.

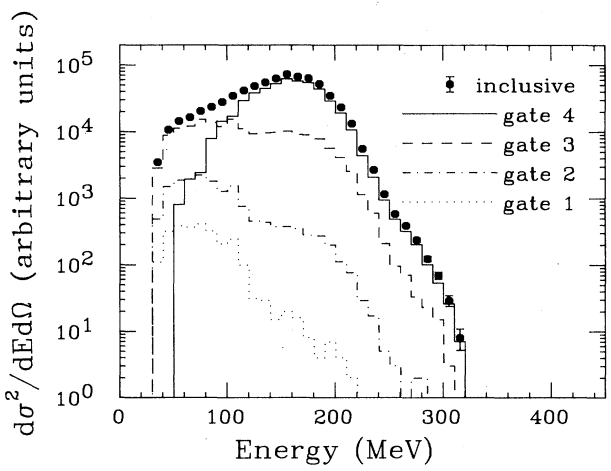

FIG. 14. Measured energy spectra of $Z=2$ particles at $\theta_{lab}=7°$ for the reaction $^{12}C+^{12}C$ at 50 MeV/nucleon gated on the midrapidity charge. The cross section is in arbitrary units.

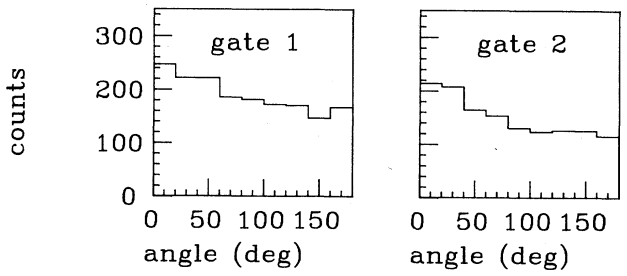

FIG. 15. The distribution of the angular difference of the vectors **Q** for two halves of each event ($^{12}C+^{12}C$ at 50 MeV/nucleon). Each distribution is gated on the midrapidity charge.

TABLE III. The gates on midrapidity charge (Z) used to select impact parameter ranges ($^{12}C+^{12}C$).

Gate	Energy (MeV/nucleon) 50
1	$Z \geq 7$
2	$5 \leq Z < 7$
3	$2 \leq Z < 5$
4	$0 \leq Z < 2$

should be strongest for the peripheral gate and should diminish with the centrality of the collision. The reaction $^{12}C+^{12}C$ at 50 MeV/nucleon has been measured with the MSU 4π array[14] and Fig. 14 shows the kinetic energy of $Z=2$ particles at $\theta_{lab}=7°$. The inclusive yield and the most peripheral gate (gate 4) show a projectilelike peak below 200 MeV. This peak diminishes in strength for gates 3 and 2, and is not present in the central collisions (gate 1). The midrapidity charge was used as the impact filter with the gates given in Table III.

To check the method used to find the reaction plane, we have divided each event from the C+C data into two halves and calculated the angular difference between the **Q** vectors of each half. In Fig. 15 we plot the distribution of this angular difference, where we have used the weightings $\omega_\nu = p_\nu^z$. This distribution has a maximum at 0° which demonstrates[8] that the method for finding the reaction plane works at these low energies. The correction factor that is used in the global transverse momentum is taken from half the width of these distributions. For these data it corresponds to $\langle \cos(\phi) \rangle \sim 0.6$.

V. CONCLUSIONS

We have examined a variety of quantities that are related to the impact parameter and the direction of the impact vector in symmetric nuclear collisions at intermediate energies. We have considered the test case of $^{40}Ca+^{40}Ca$ at 40, 70, and 100 MeV/nucleon and have used the code FREESCO to simulate the events. This renders our analysis model dependent; a problem that might be remedied by performing similar calculations with a different model which also produces real fragments. We have compared the impact parameter dependence of the multiplicity, its backward and forward components, the beam direction diagonal component of the quadrupole momentum tensor (Q_{zz}), the total perpendicular momentum, and the sum of the charge of particles at midrapidities. Two quantities, the particle multiplicity and the midrapidity charge, retain their dependence on the impact parameter after filtering through the acceptance of a typical 4π detector. By gating on these quantities we can select four ranges of impact parameters. These are distinct enough to serve as a reaction filter. The four gates produce distributions which have peaks at 0.35, 0.5, 0.7, and 1.0 b/b_{max}. The midrapidity charge has the advantage that it integrates over the final fragments and may be less sensitive to how the collision zone disassembles. For the three different energies considered here, the midrapidity charge gates sample similar

impact parameter ranges, making this quantity a filter that is suitable for excitation function experiments.

The angle of the impact vector is well reproduced with the method developed by Danielewicz and Odyniec. It was found that the weights $\omega_\nu = p_\nu^z$ give the smallest difference between the known and the found reaction plane. After filtering this difference has a half-width at half-maximum of less than 70°.

Three indirect experimental comparisons with these simulations were performed. The experimental yield of the midrapidity charge compares well to the filtered calculations of FREESCO for the system $^{40}Ar+^{51}V$ at 35 MeV/nucleon. This demonstrates that our modeling of this quantity over the full impact range is reasonable. The kinetic energy spectrum of $Z=2$ particles for peripheral collisions exhibits a projectilelike peak in the $^{12}C+^{12}C$ reaction at 50 MeV/nucleon. When the midrapidity charge gates were applied to the data, the importance of this peak diminishes with increasing centrality. This demonstrates that a simple physics expectation is borne out when this gating scheme is used. The angle of **Q** was calculated for two halves of each event for the $^{12}C+^{12}C$ data at 50 MeV/nucleon. The distribution of the difference between these angles has a peak at 0°, which demonstrates that this method will successfully find the reaction plane for the full event.

ACKNOWLEDGMENTS

The authors thank Professor Laszlo Csernai, Professor Wolgang Bauer, and Professor Pawel Danielewicz for stimulating discussions. This work was supported in part by the National Science Foundation under Grant No. PHY-86-11210.

[1]K. G. R. Doss, H. A. Gustafsson, H. H. Gutbrod, K. H. Kampert, B. Kolb, A. M. Poskanzer, H. G. Ritter, H. R. Schmidt, and H. Weiman, Phys. Rev. Lett. **57**, 302 (1986).

[2]B. B. Back, K. L. Wolf, A. C. Mignerey, C. K. Gelbke, T. C. Awes, H. Breuer, and V. E. Viola, Phys. Rev. C **22**, 1927 (1980).

[3]T. C. Awes, G. Poggi, C. K. Gelbke, B. B. Back, B. G. Glagola, H. Breuer, and V. E. Viola, Phys. Rev. C **24**, 89 (1981).

[4]M. Fatyga, K. Kwiatkowski, V. E. Viola, W. G. Wilson, M. B. Tsang, J. Pochodzalla, W. G. Lynch, C. K. Gelbke, D. J. Fields, C. B. Chitwood, Z. Chen, and T. Nayak, Phys. Rev. Lett. **58**, 2527 (1987).

[5]Z. Chen, C. K. Gelbke, J. Pochodzalla, C. B. Chitwood, D. J. Fields, W. G. Gong, W. G. Lynch, and M. B. Tsang, Nucl. Phys. **A473**, 564 (1987).

[6]K. Aleklett (private communication).

[7]K. G. R. Doss, H. A. Gustafsson, H. H. Gutbrod, B. Kolb, H. Löhner, B. Ludewigt, A. M. Poskanzer, T. Renner, H. Riedesel, H. G. Ritter, A. Warwick, and H. Wieman, Phys. Rev. C **32**, 116 (1985).

[8]P. Danielewicz and G. Odyniec, Phys. Lett. **157B**, 146 (1985).

[9]G. Fai and J. Randrup, Nucl. Puys. **A404**, 551 (1983); Comput. Phys. Commun. **42**, 385 (1986).

[10]G. F. Bertsch and S. Das Gupta, Phys. Rep. **160**, 189 (1988).

[11]M. B. Tsang, Y. D. Kim, N. Carlin, Z. Chen, R. Fox, C. K. Gelbke, W. G. Gong, W. G. Lynch, T. Murakami, T. K. Nayak, R. M. Ronningen, H. M. Xu, F. Zhu, L. Sobotka, D. Stracener, D. G. Sarantites, Z. Majka, V. Abenante, and H. Griffin, Phys. Lett. B **220**, 492 (1989).

[12]W. Bauer, Phys. Rev. Lett. **61**, 2534 (1988).

[13]G. D. Westfall, J. E. Yurkon, J. van der Plicht, Z. M. Koenig, B. V. Jacak, R. Fox, G. M. Crawley, M. R. Maier, B. E. Hasselquist, R. S. Tickle, and D. Horn, Nucl. Instrum. Methods **A238**, 347 (1985).

[14]G. D. Westfall, D. A. Cebra, J. Clayton, J. Karn, A. Vander Molen, A. Nadasen, C. A. Ogilvie, W. K. Wilson, and J. S. Winfield (unpublished).